Springer

KSME

Journal of Mechanical Science and Technology 24 (7) (2010) 1441~1449
www.springerlink.com/content/1738-494x
DOI 10.1007/s12206-010-0422-4

Flow around a freely falling square shape particle in a channel using direct-forcing fictitious domain method †

Changyoung Choi[1], Hyun-Sik Yoon[2] and Man-Yeong Ha[1,*]

[1]*School of Mechanical Engineering, Pusan National University, Jang Jeon 2-Dong, Geum Jeong Gu, Busan, 609-735, Korea*
[2]*Advanced Ship Engineering Research Center, Pusan National University, Jang Jeon 2-Dong, Geum Jeong Gu, Busan, 609-735, Korea*

(Manuscript Received December 17, 2009; Revised April 14, 2010; Accepted April 21, 2010)

Abstract

This paper presents a numerical investigation of the flow characteristics around a freely falling square shape particle in a two-dimensional channel. The FSI (fluid-solid interaction) has been realized by using the direct-forcing/fictitious domain (DF/FD) method. In order to identify the effect of fluid property on the flow characteristics and solid motion by FSI, a wide range of the fluid viscosity has been considered, which introduces various Reynolds numbers to this study. In addition, the off-centered distance of the square particle has been imposed to research the effect of the initial position. The centered particle is freely falling without rotation and transverse motion. However, the motion of the off-centered particle is significantly depended on the Reynolds number, so it is classified into the four regimes by the flow and moving characteristics of the particle. Quantitative information about the drag coefficient on the square particle is highlighted.

Keywords: Direct-forcing fictitious domain method; Drag coefficient; Flow characteristic; Freely falling particle; Square shape particle

1. Introduction

The purpose of this paper is to analysis of the flow and motion characteristics of a square shape particle by changing the fluid property and off-centered distance. The system of a two-dimensional freely falling square shape particle is the simplified case of three-dimensional particulate flows. The systems of particles immersed in a liquid or gas have many industrial and scientific applications such as chemical engineering [1, 2], fluid mechanics [3], geology [4] and biology. Some examples of these applications are petroleum industry, sandstorm, river sediment resuspension and transport, blood clogging and cell transport in arteries and veins, mixing processes when sediment-laden rivers enter lakes of the sea, powder transport by pneumatic conveying, the ticking of hour glasses, flocculation in suspensions, fluidized beds in chemical reactors, and water treatment [5, 6]. The phenomena of these systems involve the fluid-solid interaction (FSI). Therefore, the comprehension and realization of the fluid-solid interaction are essential in investigating the particulate flows.

The typical simulation methods of the particulate flows are the continuum model, discrete particle model, and direct numerical simulation (DNS) [6]. The DNS is the highest-resolution numerical method among these methods. Due to its advantage, the DNS has become more popular and many numerical schemes have been developed. Over the past decade a variety of DNS methods for the particulate flows have been proposed such as the boundary fitted grid (the adapting mesh) methods and the fixed Cartesian grid methods. Some microcosmic phenomena and mechanisms are well observed by the boundary fitted grid methods, even though it leads to tremendous computational cost. The boundary fitted grid methods have been proposed by Hu et al. [7-9] and Johnson & Tezduyar [10]. On the other hand, the fixed Cartesian grid methods require less computational cost as no need to generate new mesh and to calculate the hydrodynamics forces at each time step [11]. The fixed Cartesian grid methods have been used by Glowinski et al. [12, 13] who have presented a distributed Lagrange multiplier/fictitious domain (DLM/FD) methods. The other method for the fixed Cartesian grid methods is the direct-forcing/fictitious domain (DF/FD) method, which is suggested by Höfler & Schwarzer [5] and Yu & Shao [14]. The DF/FD method is based on the DLM/FD method and direct-forcing/immersed boundary (DF/IB) method proposed by Peskin [15]. The key idea of the DLM/FD method is that the interior domains of the particles are filled with the same fluids as the surroundings and the Lagrange multiplier (physically a pseudo body-force) is introduced to enforce the interior

† This paper was recommended for publication in revised form by Associate Editor Haecheon Choi

*Corresponding author. Tel.: +82 51 510 2440, Fax.: +82 51 515 3101
E-mail address: myha@pusan.ac.kr

(fictitious) fluids to satisfy the constraints of rigid-body motion. However, its calculation of the particle velocity and the body-force is a little more connected and expensive compared to the DF/IB method in which the no-slip condition is enforced by applying an equivalent forcing term into the Navier-Stokes equations [14].

In the DF/FD method, the body-force is calculated in the same way as the DF/IB method. However, the body-force is distributed over the particle inner domain for the constraint as a rigid-body in the DF/FD method, although in the DF/IB method, the body-force is only distributed on the particle boundary. This difference makes it possible to update particle velocities explicitly without the need of calculation of the hydrodynamic force and torque on a particle in the DF/FD method, while in the DF/IB method, the hydrodynamics force and torque should be calculated explicitly [14]. Thus, in this study, we used the DF/FD method to analysis the particulate flows for more efficient calculation.

Most of the previous numerical studies for the particulate flows have considered a circular shape particle in a two-dimensional channel [5, 8-10, 12, 13, 16-19] or a sphere particle in a tube [5, 6, 10-14, 17, 20, 21]. However, based on the survey of literature considering the similar flow conditions in terms of a square cylinder as a particle shape, only one numerical research by Wachs [22] has been found. Wachs [22] has conducted the numerical study of the falling phenomena of each shape particle at a finite Reynolds number range $\mathrm{Re} \leq 500$ by the discrete element method (DEM)-DLM/FD method and reported the results for the polygonal isometric particles (circular, square and triangle shape) in a two-dimensional channel comparing with the empirical three-dimensional results [23]. Consequently, there is little information about a freely falling square shape particle in a channel. Especially, it is hard to find that a literature has dealt with the off-centered distance of this subject.

Thus, after presenting the flow around a freely falling square shape particle in a channel which is wider than Wachs [22] in an initial stage of the paper, the main emphasis of this paper is to provide the dependence of the flow structure, the particle motion and the drag on fluid viscosity for the centered and off-centered particles.

2. Computational details

In this study, the direct-forcing/fictitious domain (DF/FD) method is used among the various schemes as mentioned in Introduction. The DF/FD method, proposed by Yu & Shao [14], is based on the distributed Lagrangian multiplier/fictitious domain (DLM/FD) method suggested by Glowinski et al. [12] and the direct-forcing/immersed boundary (DF/IB) method used by Fadlun et al. [24].

The key idea of the DLM/FD method is that the interior (fictitious) domains of objects are filled with the same fluids as the surroundings and a pseudo body-force, i.e. Lagrangian multiplier, is introduced to enforce the interior fluids in the objects to satisfy the constraint of rigid body motion [19]. However, in the DLM/FD method, the pseudo body-force is normally determined implicitly by the kinematic constraint of a solid velocity to be equal to a fluid velocity. The solid velocity can be derived from a rigid-body motion constraint in the case of a rigid object. This implicitness calculation of the pseudo body-force needs much computational cost for the interior fluids inner rigid body. On the other hand, in the DF/IB method, a no-slip boundary condition is obtained by applying an equivalent forcing term into the Navier-Stokes equations. However, under an effect of direct forcing, a velocity at the Lagrangian points on the immersed boundary may not effectively satisfy the no-slip boundary condition due to the mutual influence of the direct forcing at the nearby Eulerian nodes.

The DF/FD method has been proposed by Yu & Shao [14], which is a non-Lagrange-multiplier version of DLM/FD method without sacrificing an accuracy and robustness by employing a discrete δ (Dirac delta) -function to transfer quantities between the Eulerian nodes and Lagrangian points explicitly as the immersed boundary method. Although the DF/FD method is originated from the modification of the DLM/FD method, the body-force is calculated in essentially the same way as the DF/IB method [19]. In comparison with the DF/IB method for the particulate flows proposed by Uhlmann [17], in which the body-force is only distributed on the object boundary, in the DF/FD method, the body-force is distributed over the inner domain of the object as a constraint, which makes all inner fluids move as a rigid body. Therefore, in the DF/FD method, the time acceleration term of the inner fluids, involved in the calculation of the hydrodynamic torque on the object, does not need to be calculated explicitly.

The basic idea of the DF/FD method is that a geometrically complex domain extends to a larger simpler domain. The process of the DF/FD method suggested by Höfler & Schwarzer [5] and Yu & Shao [14] includes several calculation and interpolation steps to obtain a volume force ($\mathbf{f}$) at a location of grid point.

The momentum equation describing incompressible viscous flow for the volume force ($\mathbf{f}$) in an entire computational domain Ω_f is expressed as;

$$\frac{\partial \mathbf{u}}{\partial t} + \mathbf{u} \cdot \nabla \mathbf{u} = -\frac{1}{\rho_f} \nabla p + \nu \nabla^2 \mathbf{u} + \mathbf{f} , \tag{1}$$

where, $\mathbf{u}$ is a fluid velocity, ρ_f is a fluid density and ν is a kinematic viscosity of a fluid. The definition of a computational domain Ω_f and a fictitious domain Ω_p is shown as Fig. 1(a). To calculate the volume force ($\mathbf{f}$), Eq. (1) is transformed and discretized as follows;

$$\mathbf{f}^{n+1/2} = \frac{\mathbf{u}^{n+1} - \mathbf{u}^{n}}{\Delta t} - \mathbf{rhs}^{n+1/2} , \tag{2}$$

$$\mathbf{rhs}^{n+1/2} = -\left(\mathbf{u} \cdot \nabla \mathbf{u} + \frac{1}{\rho_f} \nabla p - \nu \nabla^2 \mathbf{u} \right)^{n+1/2} , \tag{3}$$

where, $\mathbf{u}^{n+1}$ is an unknown value in Ω_f, which is calculated by a desired velocity $\mathbf{U}_n^d$ in Ω_p. In this study, small and capital letters represent the value in Ω_f and Ω_p, respectively. The preliminary velocities in Ω_f and Ω_p are obtained by

$$\tilde{\mathbf{u}} = \mathbf{u}^n + \Delta t \cdot \mathbf{rhs}^{n+1/2}, \tag{4}$$

$$\widetilde{\mathbf{U}}(\mathbf{X}) = \sum_{\mathbf{x}\in\Omega_f} \tilde{\mathbf{u}}(\mathbf{x})\delta_h(\mathbf{x}-\mathbf{X})h^2, \tag{5}$$

where, δ_h is a discrete Dirac delta function and h is a mesh size. The discrete Dirac delta function proposed by Roma et al. [25] is introduced;

$$\delta_h(\mathbf{x}-\mathbf{X}) = \frac{1}{h^2}\phi\left(\frac{x-X}{h}\right)\phi\left(\frac{y-Y}{h}\right), \tag{6}$$

$$\phi(r) = \begin{cases} \frac{1}{6}\left(5-3|r|-\sqrt{-3(1-|r|)^2+1}\right), & 0.5 \le |r| \le 1.5 \\ \frac{1}{3}\left(1+\sqrt{-3|r|^2+1}\right), & |r| \le 0.5 \\ 0, & \textit{otherwise.} \end{cases} \tag{7}$$

The desired velocity in Ω_p is given by rigid body motion as;

$$\mathbf{U}_n^d(\mathbf{X}) = \mathbf{u}_c^n + \omega_c^n \times (\mathbf{X}-\mathbf{x}_c), \tag{8}$$

where, $\mathbf{u}_c$, ω_c and $\mathbf{x}_c$ are a translational velocity, a rotational velocity and a center coordinate of the particle. Thus we can obtain the volume force ($\mathbf{f}$) in Ω_f and the volume force ($\mathbf{F}$) in Ω_p as follows;

$$\mathbf{F}^{n+1/2}(\mathbf{X}) = \frac{\mathbf{U}_n^d(\mathbf{X}) - \widetilde{\mathbf{U}}(\mathbf{X})}{\Delta t}, \tag{9}$$

$$\mathbf{f}^{n+1/2}(\mathbf{x}) = \sum_{l=1}^{N_p} \mathbf{F}^{n+1/2}(\mathbf{X}_l)\delta_h(\mathbf{x}-\mathbf{X}_l)\Delta A_l, \tag{10}$$

where, N_p and ΔA_l are the number of forcing points in Ω_p and a discrete area corresponding to each forcing point in Ω_p. As a consequence, $\mathbf{u}^{n+1}$ can be obtained by the Eq. (2) and $\mathbf{f}^{n+1/2}$.

The DF/FD method is used to simulate a freely falling square particle. However, the DF/FD method scheme is only used for a flow field. Therefore, governing equations for the rigid-body motion are needed in the simulation of the freely falling object. First of all, the governing equations for an incompressible viscous flow are given by the momentum equation as Eq. (1) and continuity equation:

$$\nabla \cdot \mathbf{u} = 0. \tag{11}$$

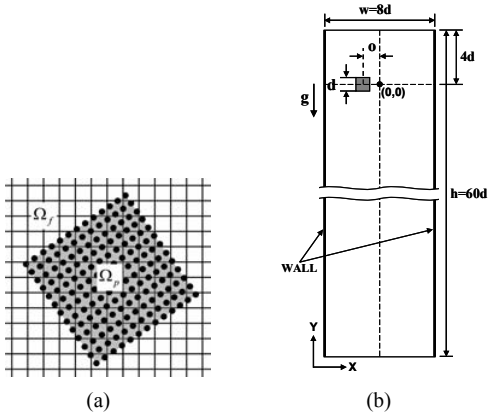

Fig. 1. Definition of the computational domain Ω_f and the fictitious domain Ω_p (a), and schematics of the system (b).

A second-order accuracy finite volume method is used for the spatial discretization in this study. The fractional step method is employed for the time advancement of the flow field. This scheme is based on the previous work of Choi & Moin [26]. Convection terms are treated explicitly using second-order Adams-Bashforth scheme, and diffusion terms are treated implicitly using Crank-Nicolson scheme.

The equation for the rigid-body motion is governed by the Newton's equation of motion defined as [14],

$$V_p(\rho_p - \rho_f)\frac{d\mathbf{u}_C}{dt} = -\rho_f \sum_{l=1}^{N_p} \mathbf{F}\Delta A_l + V_p(\rho_p - \rho_f)\mathbf{g}, \tag{12}$$

$$I_p \frac{d\omega_c}{dt} = -\frac{\rho_p \rho_f}{\rho_p - \rho_f} \sum_{l=1}^{N_p} (\mathbf{X}_l - \mathbf{x}_c) \times \mathbf{F}\Delta A_l, \tag{13}$$

where, V_p, ρ_p and I_p represent a volume, a density and the moment of inertia of the rigid-body, respectively. $\mathbf{g}$ is the gravitational acceleration.

Schematics of the system considered in a present study are shown in Fig. 1(b). The size of a channel for this study is width $8d$ and height $60d$. Initial vertical location of a particle is $4d$ from the top of the channel (d is the width of a square particle). A width of the square particle is $0.25cm$ in this work. Some dimensionless parameters are defined in this paper as,

$$W^* = w/d, \tag{14}$$

$$O^* = o/d, \tag{15}$$

where, w is a channel width and o is an off-centered distance as shown in Fig. 1(b). The off-centered particle has the non-dimensional distance O^* of 2. At the side of the channel, no-slip and no-penetration boundary conditions, $u = 0$ and $v = 0$, are enforced. The Neumann boundary condition, $\partial u_i / \partial y = 0$, is applied at the top and bottom of the channel. u_i is the velocity components in x and y directions, re-

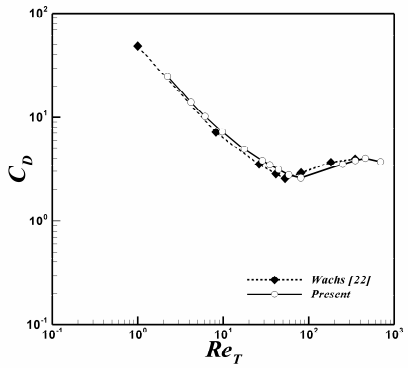

Fig. 2. Comparison of the drag coefficient as a function of the Reynolds number with the results of Wachs [22]. ($W^* = 4$, $O^* = 0.05$).

spectively. The number of total grid points is $150(x) \times 2250(y)$ for the validation case and $300(x) \times 2250(y)$ for the rest. The grids are uniformly distributed in the computational domain with mesh size $h = 1/150\,cm$. The CFL conditions for the determination of a time step are less than 0.2. Every computation for this paper is conducted up to the particle reaches bottom of the channel.

The validation of present numerical method is performed by comparison with the previous computational results by Wachs [22]. To compare the results, we modify the width of a channel in Fig. 1(b) into $w = 4d$ as Wachs [22] used. In addition to the modification of the channel width, the dimensionless off-centered distance O^* is set 0.05. Fig. 2 shows a comparison between drag coefficients of our computation and those of Wachs [22]. The drag coefficient C_D and the Reynolds number Re_T of the flow are given by

$$C_D = \frac{2F_D}{\rho_f U_T{}^2 A_p}, \tag{16}$$

$$\mathrm{Re}_T = \frac{\rho_f U_T d}{\mu}, \tag{17}$$

where, A_p is the projection surface area of the square particle, F_D is a drag force on the particle, U_T is a terminal velocity, and μ is the fluid viscosity. Since some cases for the validation do not have a steady final velocity due to the oscillation of a settling velocity, we calculate a time averaged settling velocity $\langle U_T \rangle$ suggested by Wachs [22] and use it instead of U_T .

The drag coefficients corresponding to the Reynolds number are in good agreement with the results of Wachs [22]. However, the comparison reveals the slight discrepancies between the results of the present computation and Wachs [22]'s computation. It might be carefully deducted by that the different numerical schemes have been adopted into the present and Wachs [22]'s computation.

3. Result and discussion

This work is the mimic of a sand particle sedimentation

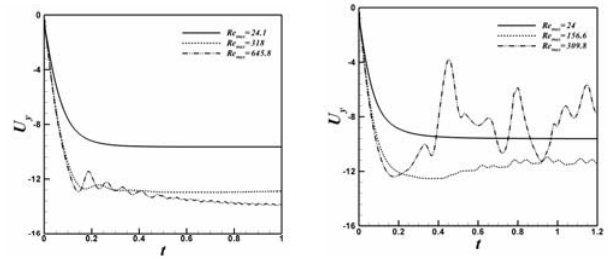

(a) (b)

Fig. 3. Settling velocity of the particle. (a) $W^* = 8, O^* = 0$, (b) $W^* = 8, O^* = 2$.

phenomenon in liquid. The density of a sand particle is about 1.2~2.0 g/cm^3 . The most common densities of the liquids (water, automobile oils, fuel oils etc.) fall into the range 0.8~1.1 g/cm^3 . Thus, in this study, we consider a density ratio ($\rho_r = \rho_p / \rho_f$, ρ_p : particle density, ρ_f : fluid density) of 1.5, and the wide range of a fluid viscosity of μ=0.005, 0.01, 0.02, 0.03, 0.04, 0.05, 0.06, 0.07, 0.1, 0.15, 0.2 and 0.25 $g/cm \cdot s$.

In this study, the settling velocity (U_y) of the particle varies significantly without any periodicity at some case as shown in especially Fig. 3(b). Therefore, the time averaged falling velocity, employed in the validation, is hard to use in results with the high-Reynolds number. Accordingly, we define the maximum Reynolds number as;

$$\mathrm{Re}_{\max} = \frac{\rho_f U_{\max} d}{\mu} \tag{18}$$

where, $U_{\max}$ is the maximum falling velocity of the particle. The reason for using the maximum Reynolds number is to avoid the effect of the large magnitude oscillation of the falling velocity and drag force at high-Reynolds number region that appears in the case of the off-centered particle with $O^* = 2$.

In the case of $O^* = 0$, the flow around the particle does not change complicatedly as shown in Fig. 4, where flow is visualized by the vorticity (ζ) normalized by the width and the maximum velocity of the square shape particle, resulting in the definition of $\zeta^* = \zeta d / U_{\max}$. Regardless of the Reynolds number, the vortex shedding in the wake does not occur with the symmetrical formation of the vortices, and the particle falls toward the bottom along the center of the channel width without the transverse motion. As the Reynolds number increases from 9.5 to 104.2, the vortices in the wake increase in size and strength, resulting in more elongation of the vortex. Consequently, the interaction between the augmented vortices and the wall shear become stronger, which can be certified by comparing with Figs. 4(a) and 4(b). Further increasing Reynolds number, the concentration of the vortices are more considerable as shown in Fig. 4(c).

It is worth to note that if the channel length considered in this study is longer, the vortex shedding in the wake might be

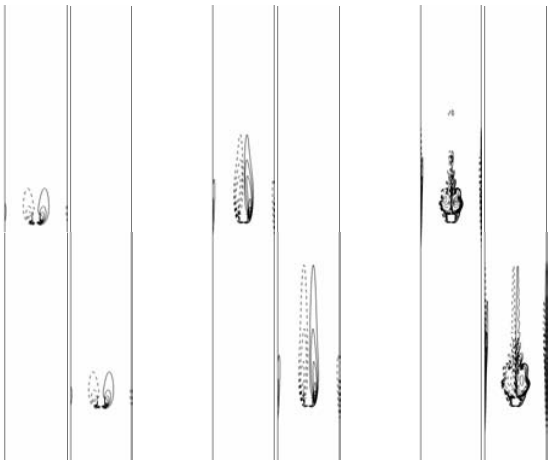

(a) $\mathrm{Re}_{\max} = 9.5$ (b) $\mathrm{Re}_{\max} = 104.2$ (c) $\mathrm{Re}_{\max} = 645.8$

Fig. 4. Instantaneous vorticity contours for some cases of $O^* = 0$. (Contour values range from -5 to 5 with 21 levels).

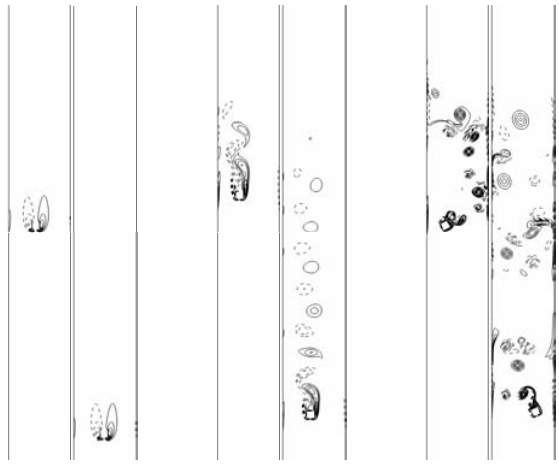

(a) $\mathrm{Re}_{\max} = 9.4$ (b) $\mathrm{Re}_{\max} = 102$ (c) $\mathrm{Re}_{\max} = 629$

Fig. 5. Instantaneous vorticity contours for some cases of $O^* = 2$. (Contour values range from -5 to 5 with 21 levels).

occurred at relatively high Reynolds numbers appearing vortex shedding under the condition of the isolated square cylinder. Thus, the present channel length is not enough for the occurrence of vortex shedding.

The initial position of the particle is shifted to the quarter of the channel width, $O^* = 2$, to see the effect of the off-centered distance. As shown in Fig. 5, the flow patterns are changed for the different maximum Reynolds number. At the low-Reynolds number region corresponding to Fig. 5(a), the flow around the particle is similar to the case of $O^* = 0$ as shown in Fig. 4(a).

When the Reynolds number increases to 102, in contrast to the case of $O^* = 0$, the vortex shedding in the wake occurs with the formation of two row of vortices as shown in Fig. 5(b), which is comparable to the wake pattern at this Reynolds number for the isolated square cylinder.

As the Reynolds number further increases, the flow pattern around the particle becomes significantly complex in Fig. 5(c). The irregular motion of the particle covering almost the width of the channel induces the wide distribution of the vortices which strongly interact with the wall shears. As a result, the various formations of vortices are originated, with the particle further falling. Moreover, those vortices are not quickly dissipated due to the small fluid viscosity where the convection is dominant to the flow.

In order to characterize the motion of the square particle, in this study, based on the falling trajectory and the rotation angle of the particle as shown in Figs. 6 and 7, respectively ($X^* = x/d$, $Y^* = y/d$, x and y are the x-directional and y-directional trajectory, respectively), motion patterns are classified into four regimes: Steady equilibrium approach, Weak oscillatory motion, Strong oscillatory motion and Irregular oscillatory motion. In this study, the transverse trajectory and rotation angle do not change at $O^* = 0$, so the classification of flow regimes are limited in $O^* = 2$.

Regarding to a circular cylinder freely falling, Feng et al. [27] have analyzed five regimes, in which the approach for the particle oscillation motion in a channel has been conducted at a different terminal settling Reynolds number. Even though the range of Reynolds number for each flow regime and some flow and motion characteristics are different, in order to unify the terminology for the definition of the flow regimes, the terminology defined by Feng et al. [27] is referred to this study.

Regime A: Steady equilibrium approach
($6.8 \le \mathrm{Re}_{\max} \le 45.9$)

In this regime, the particle is going to the center of the channel width without any oscillatory transverse motion as shown in Fig. 6(a). When the particle drifts from the initial position, the particle rotates until it approaches around the center of the channel width as shown in Fig. 7(a). As the Reynolds number increases, the rotation disappears earlier with the smaller maximum rotation angle.

Regime B: Weak oscillatory motion
($57.1 \le \mathrm{Re}_{\max} \le 73.8$)

As the Reynolds number increases in this regime, the particle is settling to the bottom of the channel with weak oscillation of the trajectory as depicted in Fig. 6(b). In the weak oscillatory motion, the particle has an unstable particle trajectory, and the rotation angle at the initial time is less than Regime A as shown in Fig. 7(b). After the particle drifts and rotates, the trajectory and rotation angle is changed with some cycle during the particle falling to the bottom of the channel. However, the particle is going to the around center of the channel width as settling.

Regime C: Strong oscillatory motion
($102 \le \mathrm{Re}_{\max} \le 156.6$)

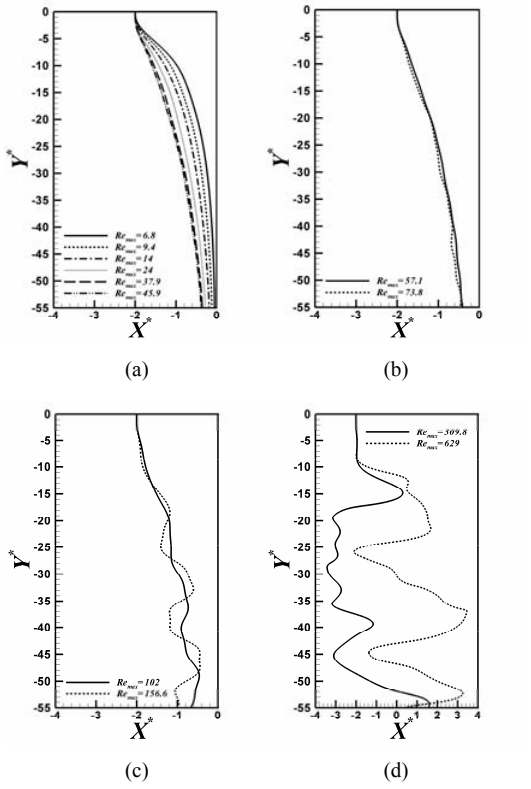

Fig. 6. Falling trajectory for each Reynolds number at $O^* = 2$.

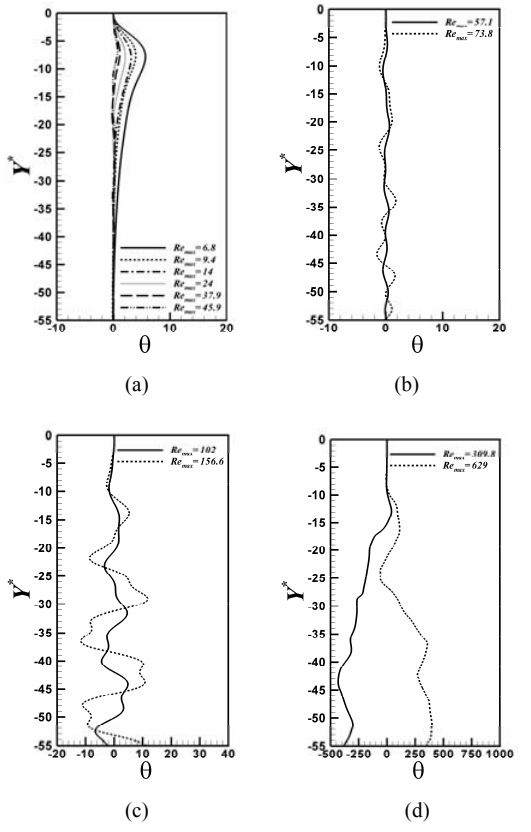

Fig. 7. Rotation angle of the particle for each Reynolds number at $O^* = 2$.

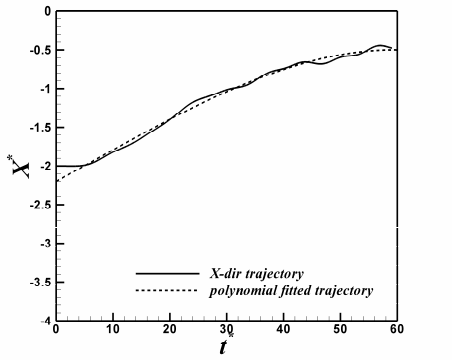

Fig. 8. X-directional dimensionless trajectory and a polynomial fitted line of $O^* = 2$, $\mathrm{Re}_{\max} = 73.8$.

The strong oscillatory motion is occurred when the maximum Reynolds number is greater than Regime B. As comparing to Regime B, the amplitude of the particle is much larger as falling to the bottom of the channel, and does not go to the center of the center of the channel as shown in Fig. 6(c). To distinguish Regime C from Regime B quantitatively, the RMS value of the x-directional deviation from the fitted trajectory, D_{RMS}, is calculated by;

$$D_{RMS} = \sqrt{\frac{\left(X^* - X^*_{fit}\right)^2}{N}}, \tag{19}$$

where, X^*_{fit} is a fitted x-directional dimensionless trajectory and N is the number of the sampling points of trajectory. The fitted trajectory is obtained by using third-order polynomial fitting equation as shown in Fig. 8 (t^* is dimensionless time which is defined as $t^* = tU_{\max}/d$). If D_{RMS} is greater than 5% of the particle width, the motion of a freely falling square cylinder is classified as Regime C. In addition to the large oscillation of the trajectory, as shown in Fig. 7(c), the magnitude of the rotation angle is larger than Regime B, however, the rotation angle changes with some periodic time as the Regime B.

Regime D: Irregular oscillatory motion
($309.8 \le \mathrm{Re}_{\max} \le 629$)

When the maximum Reynolds number is further increased, the behavior of the particle becomes unstable and brakes down into irregular patterns as Fig. 6(d). Furthermore, the rotation angle of the particle is increasing to the one direction as shown in Fig. 7(d). This phenomenon is a peculiar characteristic in this regime. The sense of rotation seems to roll down the nearby wall when the x-directional trajectory is around -3 during some time at $\mathrm{Re}_{\max} = 309.8$. However, at $\mathrm{Re}_{\max} = 629$, the x-directional trajectory is bidirectional oscillating with great magnitude, with rotation angle being slightly less than $\mathrm{Re}_{\max} = 309.8$. Therefore, in the irregular oscillatory motion, the feature of this regime cannot be defined by the specific characteristics because the particle is

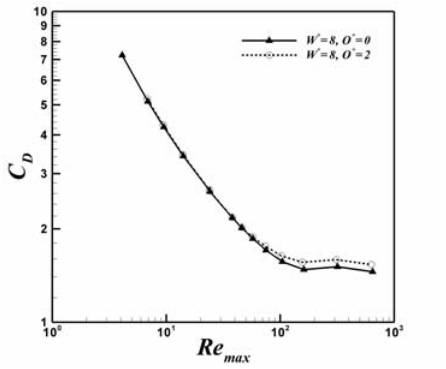

Fig. 9. Drag coefficient for a different dimensionless off-centered distance O^*.

falling and revolving without any cycle.

The drag coefficient as a function of the maximum Reynolds number for the cases of the centered and off-centered particle is shown in Fig. 9 where the effect of the off-centered distance on the drag coefficient is observed. In the low Reynolds number region corresponding to the Regime A of the particle motion, for different centered distances, the values of the drag coefficient are about the same. However, as the Reynolds number increase beyond the Regime A, the drag coefficient at $O^* = 2$ is higher than that at $O^* = 0$ .The starting maximum Reynolds number showing the drag coefficient difference between the cases of the centered and off-centered particles is consistent to that of Regime B. Because the onset of the vortex shedding deriving increment of the drag occurs only in case of the off-centered particle, the drag coefficient of the off-centered particle is larger than that of the centered particle in the range of the Reynolds number corresponding to Regimes beyond A.

4. Conclusions

In this study, the freely falling square shape particle in a channel is solved numerically by using the finite volume method. The freely falling phenomena involve the fluid-solid interaction (FSI). Accordingly, the direct-forcing/fictitious domain (DF/FD) method is used for realizing the FSI. For the verification of the present numerical method using the DF/FD method, the results are compared with those of the previous study by Wachs [22] at the same condition. The present study results by the DF/FD method agree well with the previous study ones, showing the validity of the present computation.

In order to consider the dependency of the flow around the particle and the particle motion on the fluid properties, we consider a density ratio of 1.5, and wide range of the fluid viscosity of μ=0.005, 0.01, 0.02, 0.03, 0.04, 0.05, 0.06, 0.07, 0.1, 0.15, 0.2 and 0.25 $g/cm \cdot s$. In addition to the various fluid properties, we change the initial position to see the effect of the off-centered distance as $O^* = 0$ and $O^* = 2$.

The centered particle is settling without any change for the different maximum Reynolds numbers that are induced by the fluid viscosity differences. In contrary to the isolated square cylinder, irrespective of the Reynolds number, the vortex shedding in the wake does not occur, and the particle falls toward the center of the channel width without any transverse motion due to the limitation of a channel length.

The off-centered particle, on the other hand, the particle motion is significantly depended on the Reynolds number. Thus, we classify the motion of the particle into four regimes: Regime A, B, C and D. In Regime A, the particle drifts to the center of the channel width without any oscillation, and rotates slightly until it gets to around the center of the channel width. In Regime B and C, the particle is falling to the bottom of the channel with a recurrent oscillatory transverse trajectory and rotation angle. The difference between Regime B and C is the magnitude of the oscillation of the trajectory and rotation angle is greater in Regime C. The quantitative D_{RMS} criterion of Regime B is the 5% of a particle width. Finally, in Regime D, the particle moves with an irregular pattern, so the specific feature cannot be defined.

This study also shows that the drag coefficient varies with the off-centered distance from the comparison of the drag coefficient between $O^* = 0$ and $O^* = 2$. The discrepancy of the drag coefficient between centered and off-centered particle is shown from the Regime B. Therefore, the drag coefficient difference is derived from the vortex shedding in case of the off-centered particle.

These results show that the flow and motion of a freely falling square particle are affected by the off-centered distance as well as the Reynolds number, and can be classified by the specific Reynolds number range.

Acknowledgment

This work was supported by the National Research Foundation of Korea(NRF) grant funded by the Korean Government (No.20901001302-09E0100-07110).

Nomenclature

ΔA_l : Discrete area of each forcing point
d : Particle width
$\mathbf{f}$: Volume force in computational domain
$\mathbf{F}$: Volume force in fictitious domain
$\mathbf{g}$: Gravitational acceleration
h : Mesh size
I_p : Moment of inertia of a particle
N_p : The number of forcing points in fictitious domain
o : Off-centered distance
O^* : Non-dimensional off-centered distance
$\mathbf{u}$: Fluid velocity
$\mathbf{u}_c$: Translational velocity of a particle
$\mathbf{U}_n^d$: Desired velocity in fictitious domain
V_p : Particle volume

w : Channel width
W^* : Non-dimensional channel width
$\mathbf{x}_c$: Center coordinate of a particle
δ_h : Discrete Dirac delta function
μ : Dynamic viscosity of a fluid
Ω_f : Computational domain
Ω_p : Fictitious domain
ρ_f : Fluid density
ρ_p : Particle density
ρ_r : Density ratio
ω_c : Rotational velocity of a particle
ν : Kinematic viscosity of a fluid
ζ : Vorticity

References

[1] S. L. Soo, Particulates and Continuum: Multiphase Fluid Dynamics, Hemisphere, (1989).

[2] D. Gidaspow, Multiphase Flow and Fluidization, Academic Press, (1994).

[3] E. Guazzelli and L. Oger, Mobile Particulate Systems, Kluwer Academic, (1995).

[4] K. Pye and H. Tsoar, Aeolian Sand and Sand Dunes, Unwin Hyman, (1990).

[5] K. Höfler and S. Schwarzer, Navier–Stokes simulation with constraint forces: finite-difference method for particle-laden flows and complex geometries, Phys. Rev. E, 61 (6) (2000) 7146-7160.

[6] Z. Feng and E. E. Michaelides, Proteus: a direct forcing method in the simulations of particulate flows, J. Comput. Phys., 202 (2005) 20-51.

[7] H. H. Hu, D. D. Joseph and M. J. Crochet, Direct numerical simulation of fluid particle motions, Theoret. Comput. Fluid Dyn., 3 (1992) 285-306.

[8] H. H. Hu, Direct simulation of flows of solid-liquid mixtures, Int. J. Multiphase Flows, 22 (1996) 335-352.

[9] H. H. Hu, N. A. Patankar and M. Y. Zhu, Direct numerical simulation of fluid solid systems using Arbitrary Lagrangian-Eulerian technique, J. Comput. Phys., 169 (2001) 427-462.

[10] A. A. Johnson and T. E. Tezduyar, Simulation of multiple spheres falling in a liquid-filled tube, Comput. Methods Appl. Mech. Eng., 134 (1996) 351-373.

[11] Z. Wang, J. Fan and K. Luo, Combined multi-direct forcing and immersed boundary method for simulating flows with moving particles, Int. J. Multiphase Flow, 34 (2008) 283-302.

[12] R. Glowinski, T.-W. Pan, T. I. Hesla and D. D. Joseph, A distributed Lagrange multiplier/fictitious domain method for particulate flows, Int. J. Multiphase Flow, 25 (1999) 755-794.

[13] R. Glowinski, T.-W. Pan, T. I. Helsa, D. D. Joseph and J. Periaux, A fictitious domain approach to the direct numerical simulation of incompressible viscous flow past moving rigid bodies: application to particulate flow, J. Comput. Phys., 169 (2001) 363-426.

[14] Z. Yu and X. Shao, A direct-forcing fictitious domain method for particulate flows, J. Comput. Phys., 227 (2007) 292-314.

[15] C. S. Peskin, Flow patterns around heart valves: a numerical method, J. Comput. Phys., 10 (1972) 252-271.

[16] N. A. Patankar, P. Singh, D. D. Joseph, R. Glowinski and T.-W. Pan, A new formulation of the distributed Lagrange multiplier/fictitious domain method for particulate flows, Int. J. Multiphase Flow, 26 (2000) 1509-1524.

[17] M. Uhlmann, An immersed boundary method with direct forcing for the simulation of particulate flows, J. Comput. Phys., 209 (2005) 448-476.

[18] Z. Yu, X. Shao and A. Wachs, A fictitious domain method for particulate flows with heat transfer, J. Comput. Phys., 217 (2006) 424-452.

[19] Z. Yu, A. Wachs and Y. Peysson, Numerical simulation of particle sedimentation in shear-thinning fluids with a fictitious domain method, J. Non-Newtonian Fluid Mech., 136 (2006) 126-139.

[20] N. Sharma and N. A. Patankar, A fast computation technique for the direct numerical simulation of rigid particulate flows, J. Comput. Phys., 205 (2005) 439-457.

[21] Z. Yu and A. Wachs, A fictitious domain method for dynamics simulation of particle sedimentation in Bingham fluids, J. Non-Newtonian Fluid Mech., 145 (2007) 78-91.

[22] A. Wachs, A DEM-DLM/FD method for direct numerical simulation of particulate flows: Sedimentation of polygonal isometric particle in a Newtonian fluid with collisions, Comput. Fluids, 38 (2009) 1608-1628.

[23] A. Haider and O. Levenspiel, Drag coefficient and terminal veolocity of spherical and nonspherical particles, Power Technol., 58 (1989) 63-70.

[24] E. A. Fadlun, R. Verzicco, P. Orlandi and J. Mohd-Yusof, Combined immersed boundary finite-difference methods for three-dimensional complex flow simulations, J. Comput. Phys., 161 (2000) 35-60.

[25] A. M. Roma, C. S. Peskin and M. J. Berger, An adaptive version of the immersed boundary method, J. Comput. Phys.,153 (1999) 509-534.

[26] H. Choi and P. Moin, Effects of the computational Time Step on Numerical Solutions of Turbulent Flow, J. Comput. Phys., 113 (1994) 1-4.

[27] J. Feng, H. H. Hu and D. D. Joseph, Direct simulation of initial value problems for the motion of solid bodies in a Newtonian fluid: Part 1. Sedimentation, J. Fluid Mech., 261 (1994) 95-134.

Man-Yeong Ha received his B.S. degree from Pusan National University, Korea, in 1981, M.S. degree, in 1983, from Korea Advanced Institute of Science and Technology, Korea, and Ph.D. degree from Pennsylvania State University, USA in 1990. Dr. Ha is currently a Professor at the School of Mechanical Engineering at Pusan National University in Busan, Korea. He serves as an Editor of the Journal of Mechanical Science and Technology. His research interests are focused on thermal management, computational fluid dynamics, and micro/ nano fluidics.

Changyoung Choi received his B.S. and M.S. degrees from Pusan National University, Korea, in 2008 and 2010, respectively. In his master course, he conducted many researches under the supervision of Prof. Man-Yeong Ha. His research interests are focused on flow analysis and control in turbulent flows and thermo-fluid phenomena analysis for enhancing the efficiency of the industrial devices.